PROTEINS
STRUCTURE ■ FUNCTION ■ BIOINFORMATICS

A proposed interaction mechanism between elastin-derived peptides and the elastin/laminin receptor-binding domain

G. Moroy,[1]* A. Ostuni,[2] A. Pepe,[2] A. M. Tamburro,[2] A. J. P. Alix,[1] and S. Héry-Huynh[1]*

[1] Laboratoire de Spectroscopies et Structures Biomoléculaires, Université de Reims Champagne Ardenne, IFR53, UFR Sciences Exactes et Naturelles, BP 1039, 51687 Reims Cedex 2, France

[2] Department of Chemistry, Università della Basilicata, Via N. Sauro 85, 85100 Potenza, Italy

ABSTRACT

Elastin-derived peptides (EDPs) have been intensively studied in view of their widely diverse biological activities. These are triggered both in normal and tumor cells, through peptide anchoring at the surface of the elastin-binding protein (EBP), a subunit of the elastin/laminin receptor. In this study, we investigated both the structure of the Sgal peptide, representing the elastin-binding domain of EBP, and its interaction with EDPs, through a combination of experimental and theoretical methods. Although the conformation of the Sgal peptide is highly flexible, we detected a type I β-turn at the QDEA sequence. This represents the best structured motif in the entire Sgal peptide, which might therefore contribute to its binding activity. We further propose a novel three-dimensional model for the interaction between the Sgal peptide and EDPs; folding of the EDPs at the GXXP motif, in a conformation close to a type VIII β-turn, provides the efficient contact of the protein with the Q residue of the Sgal peptide. This residue is exposed to the peptide surface, because of the β-turn structure of the QDEA residues in the peptide sequence. We further show that this complex is stabilized by three hydrogen bonds involving EDPs backbone atoms.

Proteins 2009; 76:461–476.

Key words: molecular modeling; molecular dynamics simulation; molecular docking; elastin-derived peptides; elastin/laminin receptor; elastin-binding protein.

INTRODUCTION

The extracellular matrix (ECM) is a complex environment surrounding the cells of vertebrate tissues. Elastin, one of the major fibrillar proteins of the ECM, confers elasticity and resilience to tissues undergoing important mechanic stress, such as lung, skin, or large blood vessels.[1] Elastin is a three-dimensional (3D) assembly of crosslinked tropoelastin monomers. A cell-surface receptor, the elastin/laminin receptor (ELR) mediates the insertion of tropoelastin into mature elastin in the ECM. The ELR consists of three subunits,[2] two of which, a 61 kDa neuraminidase and a 55 kDa protective protein, are inserted into the cellular membrane.[3] The third subunit, named elastin-binding protein (EBP), with a molecular weight of 67 kDa, is located at the periphery of the cellular membrane. The strong interaction between EBP and tropoelastin is characterized by a dissociation constant of 8 n*M*,[2] while EBP further contains a galacto-lectin domain. Binding of a galactosugar induces EBP conformational changes, resulting into ELR inactivation, through EBP dissociation from the other two subunits.[4]

In addition to their presence on cellular surfaces, EBP and tropoelastin also coexist in several intracellular compartments,[5] where EBP protects tropoelastin from self-aggregation and proteolytic degradation. EBP further facilitates the tropoelastin integration into the ECM,[6] and EBP recycling is required for secretion and efficient deposition of newly produced tropoelastin.[7]

Additional Supporting Information may be found in the online version of this article.

Abbreviations: 3D, three-dimensional; ABNR, adopted basis Newton–Raphson; CD, circular dichroism; EBP, elastin-binding protein; ECM, extracellular matrix; EDP, elastin-derived peptide; ELR, elastin/laminin receptor; MALDI-TOF, matrix-assisted laser desorption ionization–time-of-flight; MC, Monte Carlo; MD, molecular dynamics; MMP, matrix metalloproteinase; MT1-MMP, membrane-type 1 matrix metalloproteinase; NMR, nuclear magnetic resonance; PPII, polyproline II; PPE, porcine pancreatic elastase; RMSD, root mean square deviation; TFA, trifluoroacetic acid.

Grant sponsors: ARERS, Comité de l'Aisne contre le Cancer.
G. Moroy's current address is Laboratoire de Biophysicochimie Moléculaire, Institut de Chimie, LC3-UMR7177, Université Louis Pasteur, 4 rue Blaise Pascal, 67000 Strasbourg, France.
S. Héry-Huynh's current address is Laboratoire d'Immunologie et de Microbiologie, EA 4303 Inflammation et Immunité de l'Ephithélium Respiratoire, Université de Reims Champagne Ardenne, IFR 53, UFR de Pharmacie, 1 rue du maréchal Juin, 51096 Reims Cedex, France.
*Correspondence to: Stéphanie Hery-Huynh, Laboratoire d'Immunologie et de Microbiologie, EA 4303 Inflammation et Immunité de l'Ephithélium Respiratoire, Université de Reims Champagne Ardenne, IFR 53, UFR de Pharmacie, 1 rue du maréchal Juin, 51096 Reims Cedex, France. E-mail: stephanie.huynh@univ-reims.fr or Gautier Moroy, Laboratoire de Biophysicochimie Moléculaire, Institut de Chimie, LC3-UMR7177, Université Louis Pasteur, 4 rue Blaise Pascal, 67000 Strasbourg, France. E-mail: g.moroy@chimie.u-strasbg.fr.
Received 18 August 2008; Revised 21 November 2008; Accepted 14 December 2008
Published online 14 January 2009 in Wiley InterScience (www.interscience.wiley.com).
DOI: 10.1002/prot.22361

Under either physiological or pathological conditions, elastin can be degraded by several proteinases, including pancreatic and leukocytes elastases, matrix metalloproteinases (MMPs), and cathepsins.[8,9] The resulting elastin-derived peptides (EDPs) can interact with other ECM proteins, thereby inducing a broad range of biological activities and modification of cellular behavior.

Through their binding to EBP, EDPs containing the consensus sequence GXXPG (X being any residues) are chemotactic for numerous cells, such as macrophages,[10] leukocytes,[11] monocytes,[12] lymphocytes,[13] and fibroblasts.[14] EDPs are able to induce vasorelaxant activity,[15,16] to modify intracellular ion fluxes,[17,18] and are strongly implicated in several types of cancer. EDPs–EBP induces chemoattraction of several human tumor cells: HT-1080 fibrosarcoma,[19,20] M27 Lewis lung carcinoma,[21–23] or A-2058 melanoma[24] cell lines. Moreover, EDPs containing the GXXPG sequence induce both overexpression and activation of pro-MMP-2 at the cell surface, through their binding to EBP.[19] They are also able to upregulate the expression and secretion of pro-MMP-1 and pro-MMP-3,[25] thus modulating MMP expression. This was in turn correlated with the metastatic potential of various cancer types, including breast, colon, head and neck cancer, or melanoma.[26] It was therefore proposed that, through MMP secretion, EDPs can induce ECM proteins degradation, and thereby enhance breakdown and dissemination of cancer cells.

The interaction between EBP and EDPs has recently been demonstrated to accelerate angiogenesis, via MT1-MMP endocytosis.[27] Angiogenesis is a physiological process promoting the growth of new, from preexisting blood vessels, and contributing to spreading and growth of the tumor cells. MMPs, especially MMP-2, MMP-9, and MT1-MMP, play a major role in angiogenesis, through degradation of both ECM and vessel walls proteins, to promote formation of new capillaries from preexisting vessels.

The GXXPG sequence is shared by other ECM proteins and peptides. The study of laminin-[24] and fibrillin[28]-derived peptides showed that, when interacting with EBP, these peptides can induce biological activities, similar to those of EDPs. The GXXPG sequence was therefore proposed to be critical and to play a key role in the interaction with EBP.

Structural knowledge

Among the ELR constitutive proteins, only the 3D structure of the protective protein has been solved.[29] The 3D structures of both EBP and Neuraminidase, as well as the structural relationships between the three ELR subunits of the ELR, are still unknown.

EBP represents an inactive spliced variant of β-galactosidase, initially called Sgal.[5,30,31] It contains the VVGSPSAQDEASPLS sequence, responsible for its elastin/laminin binding properties.[5] This sequence has strong homologies with the N-terminal sequence of several serine elastases, and it was therefore proposed that these proteins might share a common ligand-binding motif. This hypothesis was supported by the observation that an antibody raised to this sequence, binds both to EBP and to porcine pancreatic elastase (PPE).[6] Moreover, the Sgal peptide, corresponding to EBP-binding sequence, retains its ability to bind to both laminin and elastin.[5,6]

Several studies were carried out to understand the relationship between EDPs structure and biological activity, using a combination of experimental and theoretical methods. Nuclear magnetic resonance (NMR) and/or circular dichroism (CD) spectroscopy did not yield accurate EDPs 3D structures.[32,33] However, we showed differences between CD spectra of active and inactive EDPs, suggesting that biological activity and structure of EDPs might be related.[34,35] On the basis of predictive calculations, we further proposed that a β-turn at the GXXP sequence might represent the active conformation.[34,36] Extensive molecular modeling was used to understand both the folding and the conformational behavior of two synthetic peptides, VGVAPG[37] and GDNP,[38] whose sequences contain the GXXP consensus motif. The results proposed that there is a dynamical equilibrium between two conformations: one characterized by a type VIII β-turn structure at GXXP, and the other by an extended structure. Molecular dynamics (MD) simulations, carried out on 128 EDPs containing the GXXP motif, demonstrated a correlation between the type VIII β-turn structure at GXXP and their biological activities.[39] This correlation was confirmed for peptides with a GXXP motif derived from fibrillin-1, an ECM protein able to upregulate MMP-1 expression and production, through EBP anchoring.[28]

In this work, we studied the Sgal peptide, using both experimental (CD and NMR spectroscopy) and theoretical methods (Monte Carlo (MC) computations and MD simulations), to unravel its structure/activity relationship. Our data suggest that a type I β-turn at the QDEA sequence represents the best structural element of this peptide, which probably contributes to its biological activity. As there is no available 3D structure for EBP, molecular docking computations were carried out using PPE as a target, as this protein shares a common binding domain to the GXXPG motif. Our results show that the PPE N-terminal sequence is the preferential binding site for all EDPs tested. In all of the lowest energy models, we identified a structural motif close to a type VIII β-turn, at the GXXP sequence of the docked peptides. Moreover, in these complexes, EDPs surround the Q residue of the receptor and form three stabilizing hydrogen bonds with the peptide elastin-binding domain. Finally, MD simulations of the PPE/VGVAPG and Sgal peptide/VGVAPG complexes demonstrated the stability of these complexes along the entire trajectories.

METHODS

Peptide synthesis and purification

The Sgal peptide was synthesized by the solid-phase procedure on an automatic synthesizer APPLIED BIOSYSTEM model 431 A. Fmoc/DCC/HOBT chemistry was used. The Fmoc amino acids were purchased from Novabiochem AG (Laufelfingen, Switzerland) and Inbios (Pozzuoli, Italy).

The peptide was detached from its resin supports using an aqueous mixture of 95% trifluoroacetic acid (TFA). It was lyophilized and purified by high-performance liquid chromatography on a semipreparative C18 reverse-phase column. Binary gradient was used and the solvents were H_2O (0.1% TFA) and CH_3CN (0.1% TFA). The purity of the peptide was assessed by matrix laser-assisted time-of-flight mass spectroscopy (MALDI-TOF).

Circular dichroism spectroscopy

The CD spectra were recorded in aqueous solution in a cylindrical cell with a 0.1 cm pathlength on a Jasco J-600 dichrograph using a HAAKE water bath as temperature controller. Peptides concentration was 0.1 mg mL^{-1}. Sixteen scans were acquired in the range 190–250 nm at a temperature of 273, 298, or 333 K by taking points every 0.1 nm, with a 20 nm min^{-1} scan rate, an integration time of 2 s, and a 1 nm bandwidth. Results were expressed in terms of $[\theta]$, the molar ellipticity in deg cm^2 $dmol^{-1}$.

Nuclear magnetic resonance spectroscopy

^1H NMR experiments were performed on a Varian Unity INOVA 500 MHz spectrometer equipped with a 5-mm triple-resonance probe and z-axial gradients. The Sgal peptide (3 m*M*) was dissolved in 700 µL of H_2O/D_2O (90/10), containing 0.1 m*M* of 3-(trimethyl-sily1)-1-propane sulfonic acid (DSS) as internal reference standard at 0 ppm. All the spectra were collected at 298 K. One-dimensional ^1H spectra were acquired with 32 K data points and a sweep width of 6000 Hz. Amide proton temperature coefficients were measured from 1D ^1H NMR spectra recorded in 5 K increments from 293 to 318 K. TOCSY spectra were collected using 256 t1 increments and a spectral width of 6000 Hz in both dimensions. Relaxation delays were set to 2.5 s and spinlock (MLEV-17) mixing time was 80 ms. ROESY data were collected essentially in the same manner as for TOCSY data, with mixing times ranging from 150 to 250 ms. The residual HDO signal was suppressed by presaturation for TOCSY; WATERGATE was used for ROESY experiments. Shifted sine bell squared weighting and zero filling to 2048 × 2048 was applied before Fourier transformation. Processing and analysis of the spectra were performed by VNMR 6.1C software (VARIAN, Palo Alto, CA). The protons resonance assignments of the peptide were straightforward achieved by standard sequential assignment procedures,[40] using a combined analysis of 2D-TOCSY and 2D-ROESY spectra. TOCSY spectra were used to identify spin systems, while ROESY allowed the assignment of resonance to individual amino acids through sequential NOE connectivities. The presence of unique amino acid residues in the peptide (G_3, Q_8, D_9, E_{10}, and L_{14}) helped for the resonance assignments, as their resonances were used as starting points in sequential NOE connectivity search.

Fluorimetric measurements of the binding of the VGVAPG to the Sgal peptide

Fluorimetric measurements were performed at 25°C on a Fluorog-3 spectrometer (Jobin Yvon/SPEX instruments) equipped with a thermoelectric temperature controller. All the data collection was performed with the DATAMAX software. As the Sgal peptide does not have a natural fluorophore, we have conserved the Fmoc group, attached to the V_1 residue during the VGVAPG synthesis. The excitation wavelength was set at 264 nm, the maximal absorption obtained in our experimental conditions. Fluorescence emission spectra were recorded in the range 280–400 nm in water in a 1-cm quartz cuvette. To determine the dissociation constant of the interaction, aliquots of Sgal in concentration ranging from 0.064 to 1.2 µ*M* were added to a solution of 13 µ*M* Fmoc-VGVAPG and fluorescence at 304 nm was measured. Nonlinear regression, one site-specific binding, was performed using GraphPad Prism version 5.00 (GraphPad Software, San Diego, CA; www.graphpad.com).

Homology modeling for the Sgal peptide

Before carrying out MC and/or MD simulations, we needed a realistic model structure of the Sgal peptide.

The initial Sgal peptide structure has been constructed from homology modeling calculations. This approach requires a 3D template structure obtained by NMR or X-ray spectroscopy at high resolution. Moreover, the template needs to share significant sequence similarity with the target protein.

Sequence homology has been previously shown between both human and ovine EBP and N-terminal part of several elastolytic serine proteases (EC: 2.3.4.*).[5,6] In Figure 1, the sequence alignments between the Sgal peptide and different serine elastases using different alignment tools (BLAST, PSI-BLAST,[41] CLUSTAL W[42]) are reported, which all give the same results.

The PPE was the protein which showed the highest sequence homology with the Sgal peptide coming from the human EBP with an identity rate of 46.15%. A high-resolution X-ray structure obtained at 0.95 Å resolution was available with the PDB code: 1GVK.[43] This structure was then used as the template to construct the Sgal

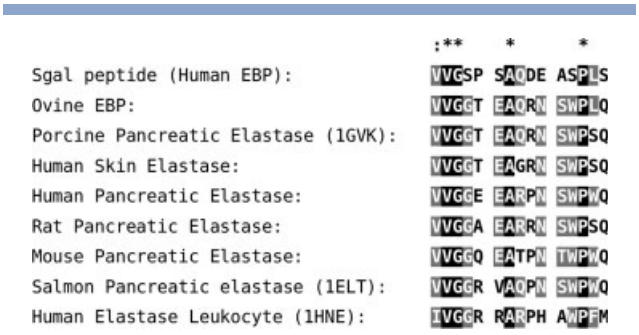

Figure 1

Multiple sequence alignment between the Sgal peptide coming from human EBP and N-terminal parts of several elastolytic serine proteases. Identical residues (*) and conservative substitutions (:) illustrate the degree of conservation between EBP and elastases. For proteins whose 3D structure has been solved, the PDB code is indicated in brackets.

peptide homology model using the Homology module of Insight98 (Molecular Simulations, San Diego, CA).

Monte Carlo simulations of the Sgal peptide

MC simulations were performed using the 4.0 version of the FANTOM (FAst Newton–Raphson TOrsion Minimizer) program.[44] The very initial structure of the Sgal peptide was the homology model obtained using the N-terminal part of PPE as a target. One hundred forty five MC runs were performed with different initial structures. Before each MC run, the structures were subjected to 100 cycles of ABNR (Adopted Basis Newton–Raphson) minimization.[45] For each run, 5000 MC steps were done for which 1, 3, or 7 torsion angles were randomly modified in the range of -180°, 180°,[46] and the corresponding structures were minimized using 120 ABNR iterations. Criterion used to accept the MC states was the one of Metropolis,[47] and an adaptative-temperature schedule protocol was employed to cross the energy barriers between local minima.[46] At the end of each run, the 10 lowest energy models obtained were clustered using a backbone root mean square deviation (RMSD) < 1 Å criterion. The lowest energy model of each cluster was then used to be the initial conformation for the subsequent MC run with different rotatable torsion angles numbers. In total, 7.5×10^5 MC steps were performed in the Sgal peptide MC simulation. During all the calculations, nonbonded interactions were truncated with a spherical cutoff of 30.0 Å. The water atomic solvation parameters used were those calculated by Efremov *et al.*[48]

Molecular dynamics simulations of the Sgal peptide and complexes

All the MD simulations were performed using the c27b3 version of the CHARMM program[49] with the potential function parameter set 22.[50] The equation of motion was solved using the Verlet algorithm with a time step of 1 fs. A 14.0 Å cutoff distance was introduced for nonbonded interaction. The van der Waals terms were multiplied by a cubic shifting function and the electrostatic terms by a cubic force switching function to smoothly reduce the potential energy between 10.0 and 12.0 Å.[51] The electrostatic interactions were treated with a dielectric constant equal to 1.0 in the presence of explicit water molecules. The peptide (or the complex) was embedded in a 47 Å $\times$ 47 Å $\times$ 47 Å (70 Å $\times$ 65 Å $\times$ 62 Å for the PPE/VGVAPG complex) equilibrated TIP3P water box.[52] Water molecules closer than 2.8 Å to any of the peptide (or complex) atoms were deleted, leading to a total number of water molecules ranging from 3.369 to 3.402 for the Sgal peptide alone (using the homology or MC model, respectively) and equal to 8.092 for the PPE/VGVAPG complex and to 3.343 for the Sgal peptide/VGVAPG complex. Periodic boundary conditions were applied.[53]

An energy minimization protocol of 100 steps of SD (steepest descent) and 400 steps of ABNR was performed on the studied system in which the solvent was fixed. The same energy minimization was used on the solvent only, whereas the peptide (or the complex) was fixed.

Finally, energy minimizations of 500 steps of SD and 3000 steps of ABNR were done without any constraint. The system was then heated up to 300 K in 30 ps and equilibrated in two 40 ps stages. In the early equilibration, velocities were assigned using a Gaussian distribution function, and in the late equilibration, the velocities were scaled every 50 steps to keep the temperature at 300 $\pm$ 10 K.

The MD simulations were systematically analyzed with the STRIDE program[54] to detect the presence of secondary structures throughout the trajectories. To classify the different types of β-turn, ϕ and ψ dihedral angles and $C\alpha_i$–$C\alpha_{i+3}$ distances were extracted from the MD simulations with the CORREL module of CHARMM. Using an R script, the Euclidean distance[39] was calculated for each quadruplet of residues to determine the β-turn type when the $C_\alpha(i)$–$C_\alpha(i+3)$ distance was lower than the usual 7 Å criterion.

Three MD simulations were performed for the Sgal peptide. The first simulation was performed using the lowest energy model obtained from the MC computations as the initial starting structure and lasted 15 ns. The two others used the homology model as the starting structure, with different initial velocities, and lasted 25 and 30 ns, respectively.

As the Sgal peptide was very flexible all along the trajectories, it appeared relevant to characterize, in the absence of regular secondary structure, the local conformation of each residue. In this aim, 10 zones of the Ramachandran map were defined, based on the regular secondary structures motifs and irregular conformations

observed in proteins.[55] The 10 zones were centered on the ideal values of the ϕ, φ dihedrals angles corresponding to the more frequently observed structures in proteins. The detection of the 10 zones was based on the extraction of the ϕ/φ dihedral angles for each residue as a function of the time, with an allowed tolerance of ±30°. It is important to note that this zone detection is unable to highlight regular structures because of the lack of information concerning other criterions, such as consecutive residues with precise ϕ/φ dihedral angles, $C\alpha_i$–$C\alpha_{i+3}$ distances for β-turns or hydrogen bond parameters.

Molecular docking

The AutoDock 3.0.5 program[56] was employed to generate an ensemble of docking conformations for each studied EDP.

The individual components of the program are AutoTors, AutoGrid, and AutoDock. AutoTors defines the degrees of freedom of the ligand, including the rotatable angles and the whole molecule rotational and translational motions.

AutoGrid precalculates a 3D grid of interaction energies based on the macromolecular target (PPE in our study). Two docking boxes were employed for each EDP. In the first one, for a blind docking step, the entire PPE was embedded in a box of 126 Å × 110 Å × 126 Å, with a 0.45 Å spacing between the grid points. All the lowest energy models for each EDP were located near the N-terminal part of PPE, the sequence having the strongest sequence homology with the Sgal peptide, and supposed to be a common elastin-binding site. More precise docking computations were then done with a 126 Å × 126 Å × 126 Å box centered on the N-terminal part of PPE, with a 0.20 Å spacing between the grid points.

Finally, docking was carried out using the AutoDock program. Four docking runs were performed using the Lamarckian genetic algorithm (LGA). A maximal number of 250 LGA runs were generated on a single population of 200 individuals. For each run, 250 independent cycles were done and set up to stop after a maximum of either 5,000,000 energy evaluations or 500,000 generations. Default parameters were used for the LGA and for the Sollis and Wet local search methods.

The studied EDPs were those for which their ability to bind to EBP and to trigger biological activities had been demonstrated[12,22,32,33]: GVAPG, GLVPG, GGVPG, VGVAPG, and PGAIPG. The EDPs were all built in a fully extended model with N and C extremities charged, using the module BIOPOLYMER of Insight98 software package (MSI, San Diego, CA). The derivation of the EDPs partial atomic charges was carried out at the AM1 level of theory as implemented in the Ampac/Mopac module of Insight98. Although the ω dihedral angles were remained fixed, all the other dihedral angles (ϕ, φ, and χ) were allowed to rotate.

RESULTS AND DISCUSSION

Experimental study of the Sgal peptide

Circular dichroism spectroscopy

CD spectra, recorded in an aqueous solution at various temperatures (see Fig. 2), show an isoelliptic point at 208 nm, indicating that the Sgal peptide in solution is in equilibrium between two conformations. These spectra are characterized by a strongly negative π–π* band, at 198 nm, which is attributed to either unordered or polyproline II (PPII) conformations. A decrease of the intensity of this band with temperature (see Fig. 2) strongly suggests that it is due to the presence of a PPII conformation.[57] The occurrence of another band at 219 nm, whose intensity becomes positive as temperature decreases, excludes the presence of a type VIII β-turn structure[38] and confirms the presence of PPII conformations.[58,59] CD spectra analysis thus provides no evidence for ordered secondary structural components, such as α-helix, β-sheet, type I or II β-turns. Instead, CD spectra demonstrate that, in water, the Sgal peptide is in equilibrium between PPII and unordered conformations.

Nuclear magnetic resonance spectroscopy

TOCSY and ROESY spectra of the Sgal peptide were recorded in water (H_2O/D_2O, 90/10) at 298 K. The NMR parameters are reported in Table I. The NOEs found are all intraresidues and sequential, thus pointing to unordered conformations. Stronger signals for sequential, than for intraresidue δαN NOEs, suggest the presence of some percentage of PPII. The absence of both sequential and medium-range δNN NOES, which excludes the pres-

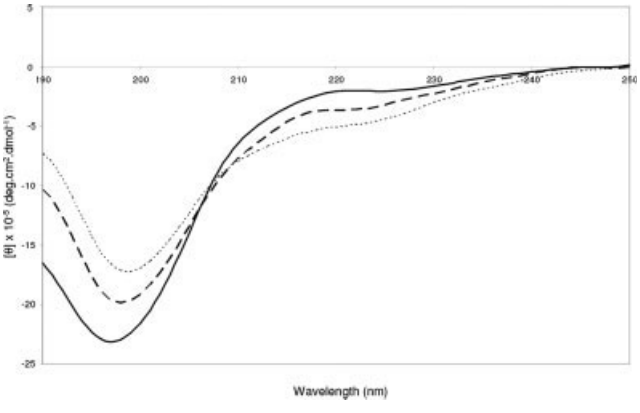

Figure 2

CD spectra of the Sgal peptide recorded at different temperatures: 273 K (–), 298 K (- - -), and 343 K (···).

ence of folded conformations in aqueous solution, also suggests some amount of PPII. The temperature coefficients of peptide amide are above to 5.2 × 10^{-3} ppb K^{-1}, suggesting that the backbone amide groups are exposed to the solvent and supporting the presence of PPII conformations. Analysis of the $^3J_{NH-H\alpha}$ coupling constants provides structural information, as these can be related to the ϕ dihedral angle using the Karplus equation,[60] except for glycine, with a single hydrogen atom sidechain. For any coupling constant, there are several solutions for the Karplus equation, such as four possible ϕ possible angles of 46.5°, 72.5°, −78.5°, and −161.0° for residue S_{12}. Residues V_2, S_6, D_9, E_{10}, and S_{15} have coupling constants compatible with two ϕ values: the first one is compatible with a PPII conformation (with angles of −83.2°, −83.2°, −83.2°, −84.7°, and −87.2° for residues V_2, S_6, D_9, E_{10}, and S_{15}, respectively), whereas the second one is compatible with a random/extended structure (with angles of −157.8°, −157.8°, −157.8°, −152.8°, and −161.0°, respectively).

Our NMR data thus suggest that the Sgal peptide, in aqueous solution, is in a PPII and/or random/extended structure conformation, indicative of a highly flexible structure for the Sgal peptide.

Theoretical study of the Sgal peptide

Homology modeling

Experimental studies demonstrated that the Sgal peptide sequence is involved in the interaction between EBP and elastin.[5,6] There are strong sequence homologies between the EBP Sgal peptide and the N-terminal part of several serine elastases (see Fig. 1). In the published elastase 3D structures,[43,61,62] the N-terminal residues are at the protein surface, and the RMSDs between N-terminal residues of different elastases are less than 0.3 Å, suggesting conservation of the N-terminal structures. These results indicate that EBP and serine elastases, with a known 3D structure, share elastin-binding motifs with sequential and structural homologies.

Among serine elastases, the N-terminal sequence of PPE has the strongest sequence homology with human EBP (46.1% identity rate). We therefore used an initial Sgal peptide structure, built by homology modeling using PPE as a template (PDB code: 1GVK[43]). The Sgal peptide homology model consists of a PPII loop at S_4PS_6, surrounded by four β-turns, defined according to Hutchinson and Thornton[63] as a type II β-turn at V_1VGS_4 and Q_8DEA_{11}, a type VIII β-turn at $E_{10}ASP_{13}$ and a type I β-turn at $S_{12}PLS_{15}$ (see Supp. Info. Fig. S1).

Monte Carlo Simulations

We performed 145 runs of MC computations in water and 73,000 structures were accepted according to the criteria described earlier (see Methods). We obtained 32 minimal energy conformations ranging from −121 to −148 kcal mol^{-1} for the lowest minimal energy conformation. All minimal energy conformations were then ranked to form structural clusters, with RMSD lower than 1 Å. Five clusters were thus obtained, which contained neither α-helix nor β-sheet secondary structures, but rather had as a common feature a structural N-terminal element consisting of four β-turns, stabilized by hydrogen bonds (Table II). These structural elements consist of three overlapping β-turns at the $V_2GSPSAQD_9$ sequence, associated with a fourth turn at $E_{10}ASP_{13}$. Two extra β-turns were detected in cluster 3 only: a type I β-turn at D_9AS_{12}, and a type II β-turn at V_1VGS_4, which induce a more compact N-terminal structure. In addition to the four β-turns common to all structures, the lowest energy model is characterized by the presence of a type I β-turn at Q_8DEA_{11}, which provides maximal exposure of the Q_8 residue to the solvent.

Table I
Proton Resonance Assignments for the Sgal Peptide in Water (90% H_2O/10% D_2O) at 298 K

Residue	Chemical shifts (ppm) NH	Hα	Hβ	Other	$^3J_{NH-H\alpha}$ (Hz)	−Δδ/ΔT (ppb K^{-1})
V_1	–	3.86	2.21	1.01	–	–
V_2	8.57	4.15	2.05	0.98	7.0	6.7
G_3	8.59	3.98	–	–	11.6	7.7
S_4	8.20	4.80	3.85	–	nd	6.6
P_5	–	4.49	2.33	2.02, 3.74/3.86	nd	nd
S_6	8.32	4.42	3.89	–	7.0	nd
A_7	8.31	4.32	1.42	–	nd	nd
Q_8	8.28	4.29	1.98/2.11	2.36	nd	nd
D_9	8.35	4.69	2.94/2.85	–	7.0	5.3
E_{10}	8.23	4.37	1.98/2.13	2.47	7.3	nd
A_{11}	8.25	4.35	1.39	–	nd	nd
S_{12}	8.26	4.78	3.85	–	6.6	nd
P_{13}	–	4.49	2.33	2.02, 3.74/3.86	nd	nd
L_{14}	8.30	4.38	1.66	1.66, 0.95/0.89	nd	nd
S_{15}	8.09	4.42	3.94/3.89	–	7.6	6.4

nd indicates values that were not determined experimentally.

Molecular dynamics simulations

The aim of the MD simulations was to detect preferential conformations of the Sgal peptide and to identify the conformation related to its binding activity. Simulations were therefore performed using various initial structures to exclude biases because of the choice of a particular initial structure. Three MD simulations were carried out in an explicit solvent, using different initial structures and different lengths of computations. The first simulation was performed using the lowest energy model obtained from the MC computations as the initial structure and lasted for 15 ns. The two other simulations used the homology model as the starting structure, with different initial velocities, and lasted for 25 and 30 ns, respectively.

Table II
β-Turn Types in the Sgal Peptide Observed in the Different Clusters of Conformations Obtained by the MC Computation

Conformation (energy in kcal mol^{-1})	β-turn types								
	V_1VGS_4	V_2GSP_5	P_5SAQ_8	S_6AQD_9	Q_8DEA_{11}	D_9EAS_{12}	$E_{10}ASP_{13}$	$A_{11}SPS_{14}$	$S_{12}PLS_{15}$
Cluster 1 (−148)		VIII	I	I	I		VIII		
Cluster 2 (−146)		VIII	I	I			VIII		
Cluster 3 (−135)	II	VIII	I	I		I	VIII		
Cluster 4 (−135)		VIII	I	I			VIII		
Cluster 5 (−134)		VIII	I	I			VIII		
Homology	II				II		VIII		I

As a comparison, the β-turns observed in the homology modeling model are indicated on the last line.

Structure analysis. The results of the three MD simulations, analyzed for secondary structures assignments using the STRIDE program,[54] show that the Sgal peptide contained neither α-helix nor β-sheet structures. A β-turns analysis was then carried out according to Hutchinson and Thornton.[63] As the Sgal peptide consists of 15 residues, 12 β-turns could be expected at most. The percentages for each type of β-turn type are given in Table III, while the β-turn distribution along the sequence and the MD trajectories is depicted on Figure 3. For each MD trajectory, β-turns, predominantly type I and type VIII, alternate with unordered conformations.

In the two first simulations, several motifs show type VIII or type I β-turn conformations with a propensity higher than 25%: $S_{12}PLS_{15}$ (51.0%), P_5SAQ_8 (45.1%), V_2GSP_5 (39.2%), S_4PSA_7 (33.6%), S_6AQD_9 (32.3%), and Q_8DEA_{11} (29.4%) for the first simulation, and P_5SAQ_8 (62.3%), S_6AQD_9 (50.8%), D_9EAS_{12} (41.6%), V_1VGS_4 (40.7%), $S_{12}PLS_{15}$ (39.5%), and Q_8DEA_{11} (29.3%) for the second simulation, respectively.

In the third MD simulation, we found only two sequences with more than 25% conformations in a β-turn: the Q_8DEA_{11} sequence with 52% conformations as β-turns (45.2% type I, 2.2% type II, and 4.6% type VIII), and the S_4PSA_7 sequence with 34.8% β-turn conformations.

In Table III, the last column summarizes the percentages for all β-turns, averaged over three simulations, with varying simulation length (weighted averages). Four sequences are predicted to have more than 25% conformations as β-turns, mainly type I: Q_8DEA_{11} (39.0%), P_5SAQ_8 (36.5%), S_6AQD_9 (29.8%), and $S_{12}PLS_{15}$ (25.7%). Moreover, in all simulations, only the Q_8DEA_{11} sequence has more than 25% conformations as β-turns.

RMSD map. To document the structural behavior of the Sgal peptide, we plotted the two-dimensional RMSD maps calculated for the backbone atoms. Such figures detect structurally close conformations during MD simulations. These conformations can be either closely related in time, yielding on-diagonal regions, or they can occur at distant times, yielding off-diagonal blocks.

The RMSD map calculated for the full Sgal peptide fails to detect close conformations during the simulation trajectories, probably because of the intrinsic flexibility of the Sgal peptide. To circumvent this problem, we focused

Table III
Percentages of β-Turn Types in the Sgal Peptide Observed During the MD Simulations

	β-turn types (% of conformations)																	
	15 ns—simulation MC (a)						25 ns—simulation HM (b)						30 ns—simulation HM (c)						All
	I	I′	II	II′	VIII	Total	I	I′	II	II′	VIII	Total	I	I′	II	II′	VIII	Total	Weighted Average
V_1VGS_4	–	–	2.4	–	–	2.4	19.0	–	13.1	–	8.6	**40.7**	0.8	–	14.5	–	6.1	21.4	24.2 ± 14.2
V_2GSP_5	–	–	–	5.0	34.2	**39.2**	–	–	–	1.3	0.7	2.0	–	–	–	3.0	3.8	6.8	12.0 ± 14.3
G_3SPS_6	–	–	–	–	–	–	–	–	–	–	–	–	–	–	–	–	–	–	–
S_4PSA_7	33.6	–	–	–	–	**33.6**	–	–	–	–	–	–	23.8	–	–	–	11.0	**34.8**	22.1 ± 16.5
P_5SAQ_8	36.1	–	–	–	9.0	**45.1**	51.8	–	–	–	10.6	**62.3**	2.0	–	–	–	8.8	10.8	**36.5 ± 23.2**
S_6AQD_9	20.4	–	0.8	–	11.1	**32.3**	43.8	–	–	–	7.0	**50.8**	5.2	–	–	–	5.9	11.1	**29.8 ± 17.6**
A_7QDE_{10}	4.4	–	–	–	0.5	4.9	1.8	–	–	–	12.0	13.7	8.9	–	–	–	2.1	11.0	10.6 ± 3.2
Q_8DEA_{11}	21.5	–	–	–	8.4	**29.4**	27.6	–	1.7	–	–	**29.3**	45.2	–	2.2	–	4.6	**52.0**	**39.0 ± 11.2**
D_9EAS_{12}	–	–	–	–	5.4	5.4	29.4	–	–	–	12.2	**41.6**	8.7	–	–	–	2.8	11.6	21.0 ± 15.5
$E_{10}ASP_{13}$	–	–	–	–	6.0	6.0	–	–	–	–	7.9	7.9	–	–	–	–	0.6	0.6	4.4 ± 3.3
$A_{11}SPL_{14}$	–	–	–	–	–	–	–	–	–	–	–	–	–	–	–	–	–	–	–
$S_{12}PLS_{15}$	44.2	–	–	–	6.8	**51.0**	30.6	–	–	–	8.9	**39.5**	0.7	–	–	–	0.8	1.6	**25.7 ± 21.3**

(a) MC—the lowest energy model from MC calculations (15 ns), (b, c) HM—the Homology Models with Different Initial Velocities (25 and 30 ns, respectively). For each simulation, the total percentage of conformations in any turn type is indicated in the last column and values higher than 25% are indicated in bold. In the very last column of the table, the average values calculated for all the turn types over all the simulations together with the corresponding standard deviations are reported.

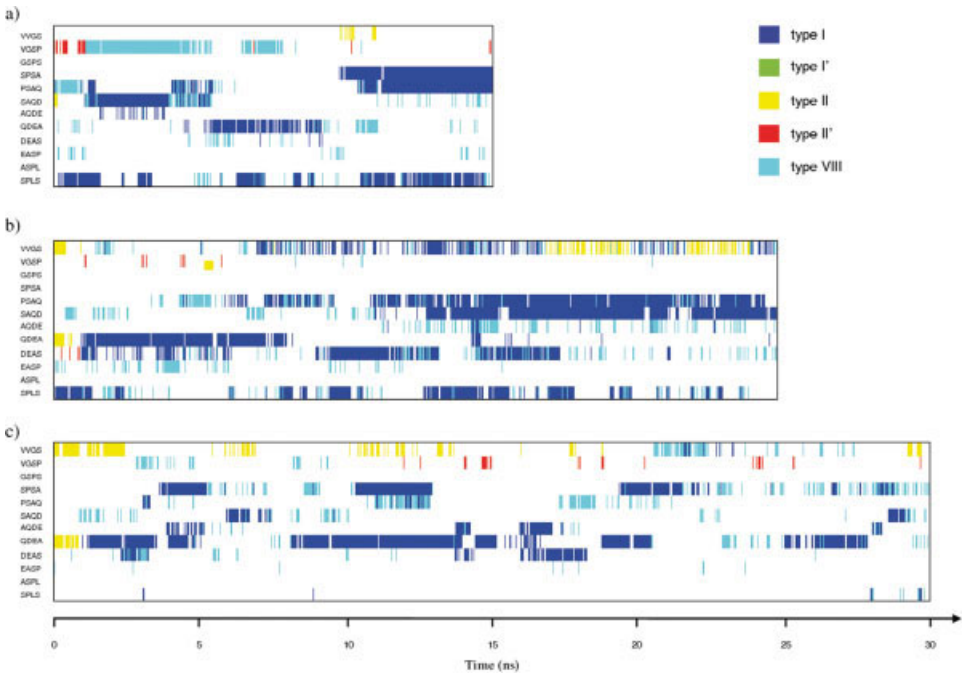

Figure 3

β-turn types occurrences for the Sgal peptide as a function of the time during the MD simulations starting from (**a**) the lowest energy model from MC calculations (15 ns), (**b**, **c**) the homology model with different initial velocities (25 and 30 ns, respectively).

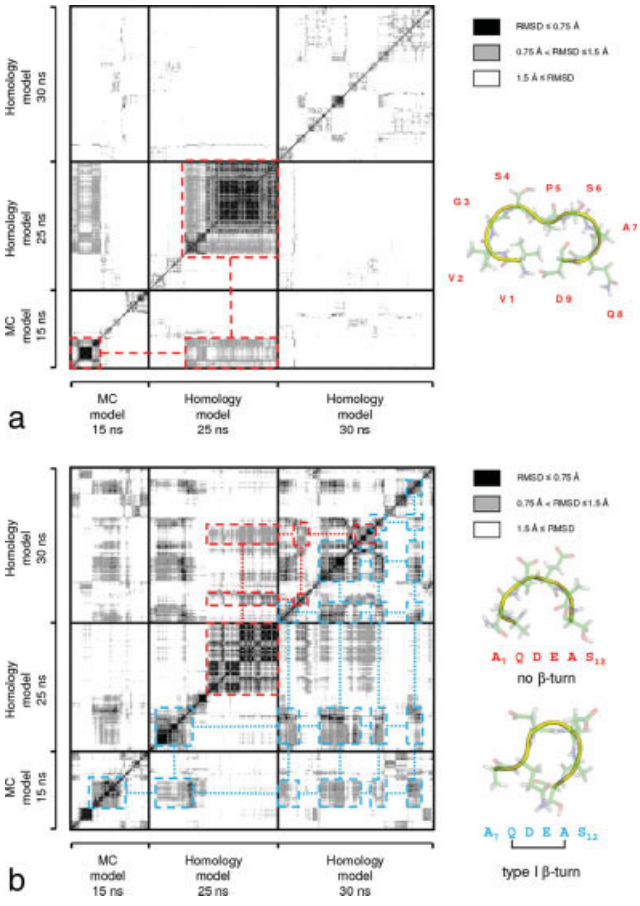

on two parts of the Sgal peptide sequence, each including one of the β-turns most frequently observed along the simulation trajectories: P_5SAQ_8 and Q_8DEA_{11}.

The P_5SAQ_8 sequence is located in the N-terminal domain, for which MC computations and MD simulations predicted many β-turns: a type VIII β-turn at V_2GSP_5 and a type I β-turn both at P_5SAQ_8 and at S_6AQD_9. We plotted the RMSD map for the N-terminal $V_1VGSPSAQD_9$ sequence of the Sgal peptide, [Fig. 4(a)]. Two diagonal blocks of close conformations appear: the first one is observed during 6 ns from the very beginning of the 15-ns trajectory (starting from the lowest energy model derived from the MC simulations), whereas the second one starts at 7 ns and lasts until the end of the 25-ns trajectory. These two blocks correspond to a single cluster of very close conformations (RMSD $<$ 1.5 Å) in both simulations, as indicated by the third (off-diagonal) block. In this cluster, the P_5SAQ_8 and S_6AQD_9 sequences

Figure 4

Backbone RMSD maps for the Sgal peptide simulations restricted to (**a**) the $V_1VGSPSAQD_9$ sequence and (**b**) the A_7QDEAS_{12} sequence. Are indicated by colored squares clusters of close conformations, and the corresponding average conformation is represented on the right. For the second map (b), regions in red are corresponding to a cluster of conformations, which do not exhibit any turn but rather extended/unordered structures, and regions in blue correspond to a cluster of conformations showing a type I β-turn on Q_8DEA_{11}.

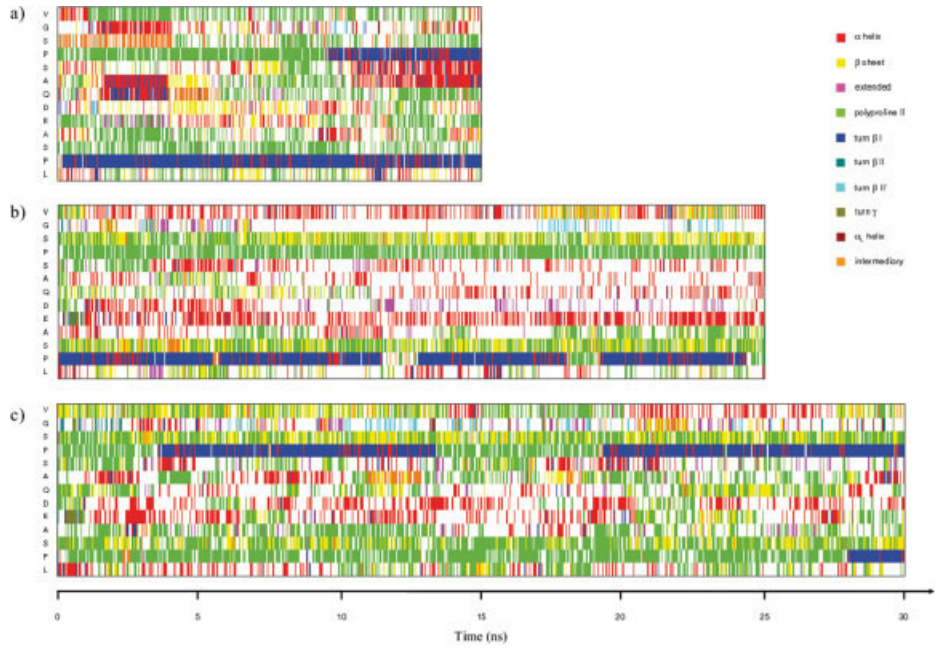

Figure 5

ϕ/φ visited zones as a function of the time for each residue constituting the Sgal peptide during the MD simulations starting from (**a**) the lowest energy model from MC calculations (15 ns), (**b**, **c**) the homology model with different initial velocities (25 and 30 ns, respectively).

are folded in type I β-turns, as expected, but no β-turn appears at V_2GSP_5. However, another β-turn occurs at V_1VGS_4, on average in 21.5% of the conformations obtained during the three MD simulations. This structural motif, formed by three β-turns at V_1VGS_4, P_5SAQ_8, and S_6AQD_9, is close to that observed in cluster 5 given by MC computations.

The Q_8DEA_{11} sequence has both the highest propensity to fold as a β-turn, and in all the simulations, is predicted to have more than 25% conformations as type I β-turns. We plotted the RMSD map for this sequence, extended by adding one N- and one C-terminal residue, that is, the A_7QDEAS_{12} sequence [Fig. 4(b)]. Two major clusters of close conformations appear from the three MD simulations. The first cluster, marked in red, shows mostly during the second simulation and briefly during the third one. The corresponding conformations contain no defined secondary structure elements, but rather consist of unordered/extended structures. The second cluster of close conformations, indicated in blue, is frequently observed in all the simulations. The conformations in this cluster include a β-turn at Q_8DEA_{11}, mainly of type I but also of type VIII (Table III).

The results of the above simulations carried out on the Sgal peptide thus suggest the occurrence of β-turns at equilibrium with more extended/unordered conformations. These data emphasize the significance of the β-turn at the Q_8DEA_{11} sequence, as it corresponds to the most frequent secondary structure motif detected during the MD simulations, it fits the lowest energy model obtained by MC computations and it is also found in the homology model. Although these results stress the importance of the Q_8DEA_{11} β-turn as a structural element possibly involved in protein binding, these differ from our previous experimental data, more suggestive of an equilibrium between unordered and PPII conformations. A more detailed study of the conformations observed during simulations was therefore undertaken to analyze the behavior of each residue of the Sgal peptide sequence.

Analysis by ϕ/φ dihedral angles zones. After analysis of the three MD trajectories in terms of the Ramachandran's map zones occupancy, we plotted on Figure 5 the different zones explored by each residue as a function of time for each simulation. The percentages of each visited zone, averaged for all conformations and for all residues, are listed in Table IV, for each MD trajectory.

These results indicate that for each residue and in each simulation, the most populated region is that of PPII, with occupancy percentages of 23.6, 17.7, and 28.6% for simulation 1, 2, and 3, respectively. The S_4 and S_{12} serine residues, each followed by a proline, show preferential and stabile occupancy of the β-sheet and PPII zones, in agreement with the behavior of proline residues in proteins.[64]

The second most highly populated zone is the α-helix, whereas we rather expected the type I β-turn zone. This

Table IV
Percentages of occupancy of the different Ramachandran's map zones averaged over all the residues constituting the Sgal peptide and over all the conformations explored during the different trajectories

	Zones	% occupancy	Zones	% occupancy
(a) MC—15 ns	α Helix	11.7	Type II β turn	0.1
	β Sheet	4.8	Type II′ β turn	0.2
	Extended	1.2	γ Turn	0.1
	Polyproline II	23.6	α_L Helix	0.1
	Type I β turn	11.1	Intermediary	3.7
Outside the zones		43.4		
(b) HM—25 ns	α Helix	13.0	Type II β turn	0.2
	β Sheet	9.9	Type II′ β turn	0.5
	Extended	1.5	γ Turn	0.2
	Polyproline II	17.7	α_L Helix	0.1
	Type I β turn	6.5	Intermediary	1.2
Outside the zones		49.2		
(c) HM—30 ns	α Helix	9.7	Type II β turn	0.2
	β Sheet	9.8	Type II′ β turn	0.5
	Extended	1.4	γ Turn	0.3
	Polyproline II	28.6	α_L Helix	0.1
	Type I β turn	5.9	Intermediary	1.4
Outside the zones		42.1		

(a) The lowest energy model from MC calculations (15 ns), (b, c) the homology models with different initial velocities (25 and 30 ns, respectively).

can be accounted for by to two major factors, one because of the intrinsic structural features of the type I β-turn. A type I β-turn structure is constituted by four consecutive residues in which the $i + 1$ residue and $i + 2$ residues have dihedral angles values corresponding to the α-helix and type I β-turn zones, respectively. The second factor accounting for this discrepancy is the overlap between zones corresponding to an α-helix ($-60°$; $-40°$) and to a type I β-turn ($-90°$; $0°$), given the allowed tolerance of $\pm 30°$. For example, a residue with φ/ψ angles of $-70°/-30°$, which actually belongs to a type I β-turn conformation, might be wrongly assigned to an α-helix, because its dihedral angles are closer to an α-helix than to a type I β-turn. Many residues which appear in the α-helix zone thus actually belong to a type I β-turn conformation.

In the course of these simulations, more than 40% of all residues were found in poorly defined zones, corresponding to unordered structures.

Comparison between experimental and theoretical results. CD and NMR spectroscopy data indicated that, in an aqueous solution, the Sgal peptide structure is a mixture of random coil and PPII conformations. These data do not mean that the Sgal peptide is helical, but rather that the dihedral angles of many residues are compatible with a PPII structure. As NMR or CD spectroscopy measurements provide a time-average of all peptide conformations in solution, these techniques fail at characterizing the Sgal peptide structure, as observed for flexible molecules.

Computational methods are therefore helpful for a better characterization of flexible peptides in solution and can complement experimental data. We used two complementary approaches: MC and MD simulations. The MD dynamics simulation provides a structural analysis of the system as a function of time. The MC method, being a time-independent method, is not suited for the study of the dynamical behavior of the Sgal peptide. It can however prove useful to explore the conformational space and sample the Sgal peptide accessible conformations, through crossing of energetic barriers, not accessible through MD simulations. The lowest energy model obtained by MC simulation is characterized by five β-turns, including a type I β-turn at the QDEA sequence. Differences between this structure and that obtained from experimental might be due to limitations of the MC method. Although we carried out a large number of iterations, coupled to an adaptative-temperature schedule protocol, and analyzed a large number of structures, we have no certainty about reaching the global minimum. Moreover, the implicit solvation model we used might have induced some protein and peptide structural collapse. The above results obtained by MC and MD methods are thus in good agreement, especially in suggesting a type I β-turn at the Q_8DEA_{11} sequence.

Replica exchange molecular dynamics (REMD) simulations[65] were performed to obtain additional data on the Sgal peptide structure. This method enables efficient simulation at a given time, and at different temperatures, of various biological systems. β-turn analysis of four independent REMD trajectories identify the Q_8DEA_{11} type I β-turn, as the most frequently observed secondary structure motif for the Sgal peptide (see Supp. Info. Table SI). These data thus further support the hypothesis that this β-turn might be central to the binding of the Sgal peptide (or EBP) to the EDPs.

The analysis of the Ramachandran's map zones occupied by peptide residues during MD simulations can be related to the structural and dynamical behavior of the Sgal peptide predicted from experimental techniques. This analysis showed that the Sgal peptide residues occupy mainly zones corresponding to undefined/unordered or PPII structures, in agreement with our experimental results.

Although a type I β-turn at the Q_8 DEA_{11} sequence is the most frequent secondary structure detected during the MD simulations, it appears only in 36.9% of the MD conformations, and it is not detected in the CD spectra. However, as other extended and unordered structures coexist with that turn in the Sgal peptide, the characteristic signal for that turn is probably too weak to be clearly detected in the CD spectra.

The NMR experiments failed to identify a β-turn at the Q_8DEA_{11} sequence. However, a comparison of the $^3J_{NH-H\alpha}$ values for the central residues in the turn, glutamic acid D_9 and aspartic acid $E_{10,}$ with the results obtained from MD simulations, shows that these values are compatible with ϕ dihedral angle values of $-157.8°$

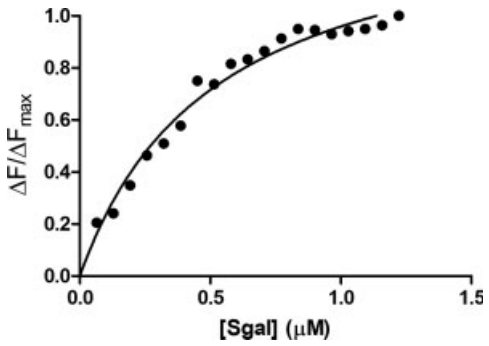

Figure 6
Characterization of the VGVAPG-Sgal peptide interaction.

or −83.2° and −152.8° or −84.7°, respectively. The second values for each residue are similar to those of a classical type I β-turn, with central ϕ dihedral angles of −60.0° and −90.0°, respectively. The NMR experiments thus support a type I β-turn at Q_8DEA_{11}.

Interaction between the Sgal peptide and EDPs

Binding of the Sgal peptide to tropoelastin is well characterized,[6] whereas direct binding of the Sgal peptide to EDPs has not been demonstrated yet. To address this question, we studied experimentally the affinity of the Sgal peptide for the VGVAPG elastin-derived hexapeptide. The VGVAPG was selected as one of the most studied EDP widely used to explore EDPs biological activities.[9,25,66] Molecular docking computations of several EDPs were then performed to investigate the structural requirements for EDPs anchoring to the elastin-binding domain. As no EBP 3D structure was available, we have chosen the PPE as a target, as it shares with EBP a common elastin-binding domain. The VGVAPG structure of the lowest energy docking model was then used to study its interaction with the Sgal peptide, by transposing PPE docked structure onto the Sgal peptide. The stability of two relevant complexes (VGVAPG/PPE and VGVAPG/Sgal peptide) was finally analyzed through MD simulations in explicit water.

Sgal peptide/VGVAPG affinity measurements

To investigate a possible interaction between the VGVAPG and Sgal peptides, we monitored the changes in fluorescence of the Fmoc-VGVAPG peptide upon addition of the Sgal peptide.

The maximal emission wavelength of Fmoc-VGVAPG was at 302 nm. Addition of the Sgal peptide shifted the emission maximum toward 304 nm and significant fluorescence quenching was observed (data not shown). The decrease in fluorescence intensity at 304 nm upon addition of increasing concentrations of the Sgal peptide enabled the calculation of a K_d value of 515 n*M* (±59 standard error) (see Fig. 6).

PPE/EDPs docking calculations

As described earlier, we used the 3D PPE structure to mimic local EBP behavior and study the interaction between EBP and EDPs. Several molecular docking calculations were performed between PPE as a target, and EDPs containing GXXPG sequences which are either able (VGVAPG, PGAIPG, GVAPG, GLVPG) or unable (GGVPG) to bind EBP.[22,32,33]

The optimal solutions obtained from blind docking all suggest that for each EDP, the binding domain belongs to the N-terminal part of the PPE sequence, which is highly homologous to the Sgal peptide sequence. The conformation of all EDPs is characterized by a distorted type VIII β-turn at GXXP (Table V), as the distance between the first and fourth residues of the turn is slightly above 7 Å. The β-turn at the EDPs GXXP sequence surrounds the Q_8 residue of PPE, and the interaction between the two molecules is stabilized by three hydrogen bonds as shown on Figure 7: (PPE-Q_8) NH···C=O (X_2), (PPE-E_6) C=O···NH (X_2), and (PPE-E_6) C=O···NH (X_1). As these hydrogen bonds involve backbone atoms, it suggests that the interaction is independent of the nature of the EDPs residues. The EDPs atoms involved in those H-bonds (X_2-C=O, X_2-NH, and X_1-NH) all point toward the same direction. This geometry is characteristic of a type VIII β-turn, as no other β-turn type on GXXP has a similar 3D configuration. Van der Waals interactions between PPE and EDPs residues were also observed. The PPE residues involved are mainly located in the sequence corresponding to the Sgal peptide (residue number <15), supporting the hypothesis that this sequence represents the elastin-binding site. Among these residues, the X residue preceding the GXXP motif

Table V
Structural Characteristics of the GXXP Motifs in the Best PPE/EDPs Molecular Docking Models

EDP sequence (X)**GX$_1$X$_2$PG**	X_1 residue		X_2 residue		C_α(G)–C_α(P) distance (Å)
	ϕ (°)	ψ (°)	ϕ (°)	ψ (°)	
V**GVAP**G	−112.3	−38.6	−117.3	127.6	7.2
P**GAIP**G	−115.6	−45.9	−138.6	114.5	7.8
GVAPG	−98.5	−52.8	−128.1	119.1	7.3
GLVPG	−103.5	−64.5	−133.5	142.8	7.5
GGVPG	−93.0	−65.0	−124.5	132.5	7.3

For record, β-turns are defined as four consecutive residues for which C_α–C_α distance between residues 1 and 4 (designed by i and $i + 3$) is lower than 7 Å. β-turns can then be grouped according to their backbone ϕ, ψ dihedral angles into seven structural types (I, I′, II, II′, VIa, VIb, and VIII) with an allowed tolerance of ±30.0° for three angles and ± 40.0° for the fourth one. As an example, type VIII β-turns are defined by: $\phi(i+1) = -60.0°$, $\psi(i+1) = -30.0°$, $\phi(i+2) = -120.0°$, $\psi(i+2) = -120.0°$. The EDPs structures here obtained are all corresponding to distorted β-turns, as the C_α(G)–C_α(P) distance is slightly above the criterion, with ϕ, ψ angles values close to those of a type VIII β-turn.

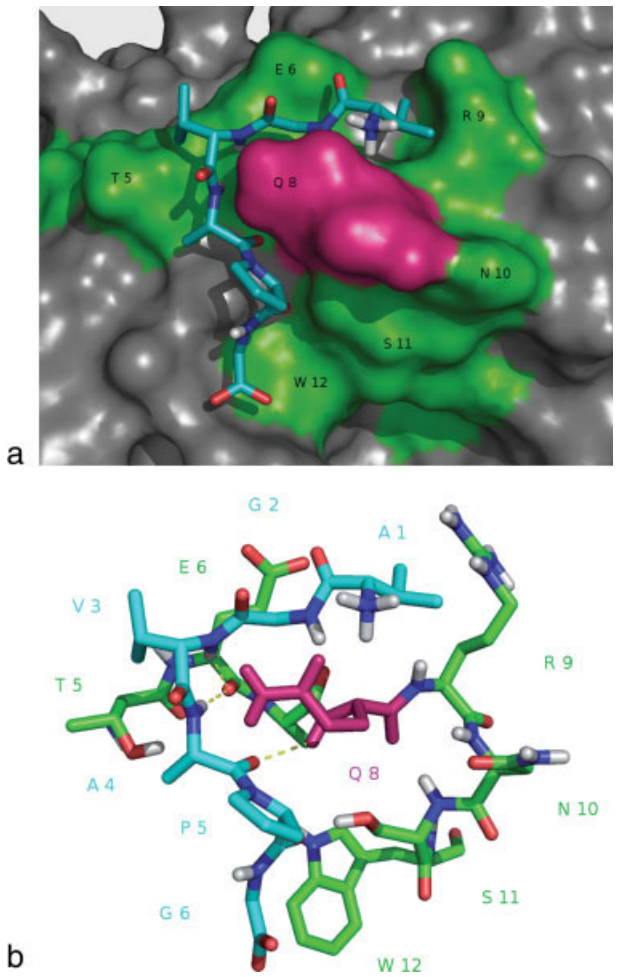

Figure 7

Representation of the PPE/VGVAPG complex obtained by docking calculations. (**a**) PPE is represented by its accessible surface in gray, and the Sgal-corresponding sequence in green, with the Q_8 residue pointing out to the solvent in pink. VGVAPG, represented in sticks and colored in cyan, is wrapped around the Q_8 residue. (**b**) Are highlighted in yellow dashed lines the three hydrogen bonds between VGVAPG and E_6 and Q_8 residues of PPE (represented in green).

interacts with E_6, A_7, Q_8, R_9, and H_{60}; the glycine residue of the GXXP motif interacts with E_6, A_7, and Q_8; the central X_1 and X_2 residues interact with T_5, E_6, Q_8 and with T_5, E_6, A_8, Q_9, and Q_{147}, respectively; the proline residue of the GXXP motif interacts with S_{11}, W_{12}, and Q_{147}; finally, the glycine residue, following the GXXP motif, interacts with W_{12}, Y_{128}, and Y_{200}. This glycine residue is required for the EDPs activity.[25] According to our docking results, the glycine residue following the GXXP motif lies in a small pocket formed by the W_{12}, Y_{128}, and Q_{147} residues. Although we cannot fully account for contribution of this glycine to the interaction, our data suggest that a short sidechain residue following the GXXP sequence might help EDPs anchoring.

According to our computations, binding of the inactive GGVPG peptide[33] to PPE is similar to that of the active peptides. Our previous data[39] showed that the inactive GGVPG peptide, as any peptide containing the GXXP motif, can fold in a type VIII β-turn structure. Among all peptides studied, only this one could also fold in a type II′ β-turn. We then proposed that its inactivity was due to its dynamical properties and more specifically to its ability to switch from a β-turn type to another.[39] Docking methods cannot select peptides on dynamical behavior or intrinsic flexibility, but our data confirmed that a peptide containing the GXXP sequence preferential folds as a type VIII β-turn and binds to the N-terminal part of PPE sequence, which has strong homology with the Sgal peptide.

Docking calculations further stressed the importance of the Q_8 residue for EDP anchoring, as it is exposed to the solvent and thus promotes interaction of the type VIII β-turn at GXXP, with its sidechain. This interaction is stabilized by van der Waals contacts and by a hydrogen bond between the Q_8 backbone amide hydrogen atom and the proline backbone carbonyl group of the GXXP sequence. Conservation of the Q_8 residue between serine elastase sequences, or its replacement by another hydrophilic residue (see Fig. 1), further supports the importance of glutamate Q8. As the E_6 residue is also involved in hydrogen bonding and in van der Waals interactions with EDPs, it is probably, albeit in a nonspecific way, as the hydrogen bonds are between backbone and not sidechain atoms.

We performed similar docking calculations using the EADock[67] program based upon the CHARMM 22 forcefield (data not shown). The lowest energy models obtained for EDPs were similar to those generated by the AutoDock computations, with a RMSD for heavy atoms between 1.0 and 1.7 Å. Specific features for this interaction, including a distorted type VIII β-turn at GVAP, surrounding the PPE Q_8 residue, as well as the stabilizing hydrogen bonds, are conserved, thus supporting the binding model proposed here.

Molecular dynamics simulation of the PPE/VGVAPG complex

To test the stability of the docked models, we studied the dynamic behavior of the PPE/VGVAPG complex, through a 4 ns MD simulation, in explicit aqueous solvent. We selected the VGVAPG EDP, as it has a wide range of biological activities, and has been thoroughly characterized both experimentally and theoretically.

No significant secondary structure modifications were detected during the trajectory. We focused on the N-terminal part of PPE, the $V_1VGGTEAQRNSWPSQ_{15}$ sequence corresponding to the Sgal peptide and strongly interacting with VGVAPG. Initially, one PPII loop was present at G_4TE_6 and five β-turns of type II, type I, type

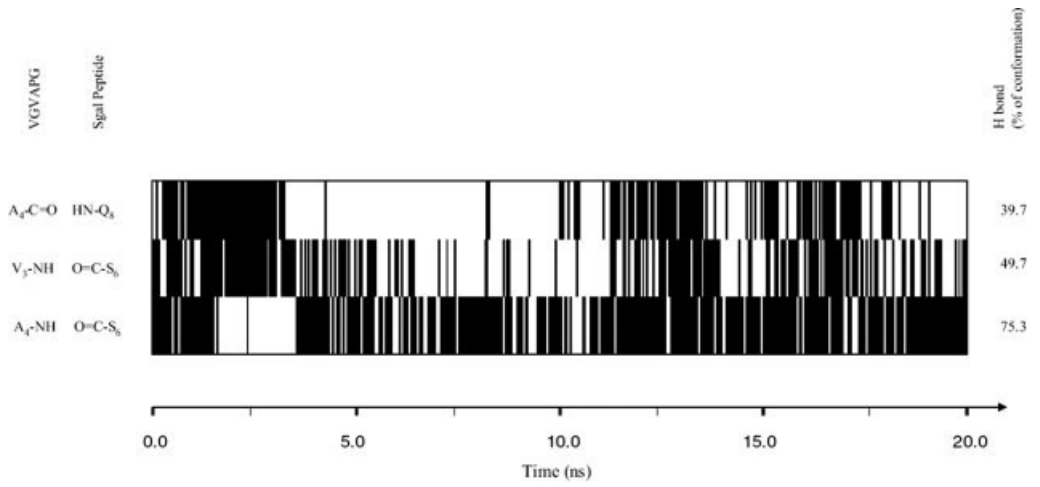

Figure 8

Hydrogen bond occurrences (black sticks) as a function of time during the MD simulation of the Sgal peptide/VGVAPG complex.

I, type VIII, and type I were observed at V_1VGG_4, Q_8RNS_{11}, R_9NSW_{12}, $N_{10}SWP_{13}$, and $W_{12}PSQ_{15}$, respectively. Only the type I β-turn at R_9NSW_{12} disappeared after 1.7 ns, whereas the others remained unchanged during the entire trajectory. The VGVAPG peptide keeps a distorted type VIII β-turn structure along the MD simulation with a average C_α (G)–C_α (P) distance of 7.5 Å, with an average backbone RMSD below 1.0 Å. No β-turn was detected at either VGVA or VAPG. Three hydrogen bonds were identified between PPE and VGVAPG, in the initial molecular docking model. The (PPE-Q_8) N—H···C=O (X_2) hydrogen bond is disrupted at the beginning of the trajectory while the (PPE-E_6) C=O···N—H (A_4) and (PPE-E_6) C=0···N—H (V_3) bonds were observed in, respectively, 50.6 and 95.8% of the conformations. The interaction between PPE and VGVAPG is therefore conserved along the 4-ns trajectory, as two of three hydrogen bonds remain unchanged during the trajectory, and no significant structural change occurs.

Molecular dynamics simulation of the Sgal peptide/VGVAPG complex

The structure obtained by molecular docking calculations of the PPE/VGVAPG complex was used for the study of the Sgal peptide/VGVAPG complex stability. The lowest energy model derived from the AutoDock program for VGVAPG docked to PPE was presented to the Sgal peptide, whose initial structure was calculated by homology modeling. The relative orientations were identical to those obtained for the PPE/VGVAPG complex after docking calculations. We then performed a 20 ns MD simulation in explicit aqueous solution.

Three H-bonds are observed in the VGVAPG/Sgal peptide complex: (Sgal-Q_8) N—H···C=O (A_4), (Sgal-S_6) C=O···N—H (V_3), and (Sgal-S_6) C=O···N—H (A_4). These hydrogen bonds are similar to those observed in the VGVAPG/PPE complex and are observed along the trajectory in, respectively, 39.7, 49.7, and 75.3% of the sampled conformations (see Fig. 8). The persistence of these hydrogen bonds indicates that the VGVAPG EDP interacts with the Sgal peptide during at least 20 ns, suggesting that the proposed conformation is the binding conformation.

As in the MD simulations of the Sgal peptide alone in solution, in the complex, the peptide contains several β-turns (Fig. 9 and Table VI). However, the QDEA motif appears as a β-turn in only 9.4% of the sampled conformations. The β-turn at QDEA is observed at the beginning of the trajectory, up to 4.0 ns. After 4.0 ns, the C_α–C_α distance between Q_8 and A_{11} increases slightly above 7 Å, and it is therefore no longer assigned to a classical β-turn structure. On the contrary, the VGVAPG peptide, which did not appear as a classical type VIII β-turn structure in the PPE/VGVAPG docked model, folds into a type VIII β-turn at GVAP during the trajectory, as 28.6% of the sampled conformations show this structural motif (Fig. 9 and Table VI). This β-turn wraps around the Q_8 residue of the Sgal peptide and enables formation of three hydrogen bonds between the Sgal peptide and VGVAPG, as described earlier. Furthermore, a type I or II′ β-turn is also observed at the VGVA motif, mainly halfway the MD simulation. This kind of overlapped β-turns on EDPs was previously observed during MD of EDPs alone in solution.[39] On the contrary, no β-turn was detected on VAPG.

The results of the MD simulation of the Sgal peptide/VGVAPG complex thus show that the stability of the

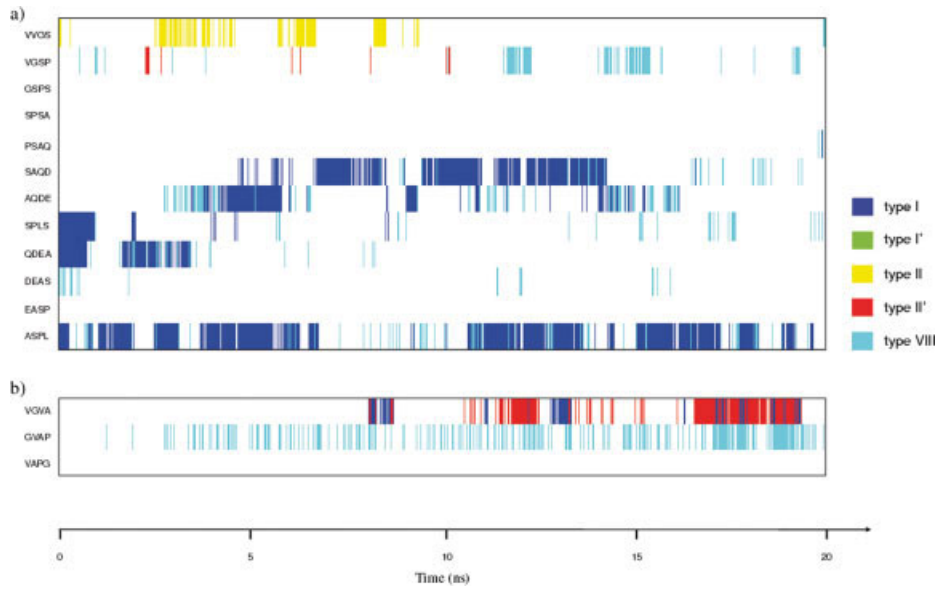

Figure 9

β-turn types occurrences as a function of time during the MD simulation of the Sgal peptide (**a**)/VGVAPG (**b**) complex.

complex is provided through three hydrogen bonds involving VGVAPG backbone atoms. A type VIII β-turn on GVAP wraps around the Sgal peptide Q_8 residue, well-exposed to the solvent through a conformation close to a type I β-turn structure at the QDEA sequence. This interaction structure supports the previous assumption that a type VIII β-turn on GXXP is required for anchoring EDPs onto EBP.[25,35,39]

Table VI

Percentages of β-Turn Types Observed During the Sgal Peptide/VGVAPG Complex Trajectory (20 ns)

	β-Turn types (% of conformations)					
	I	I′	II	II′	VIII	Total
Sgal peptide						
V_1VGS_4	–	–	12.9	–	0.2	13.1
V_2GSP_5	–	–	–	1.3	8.7	10.0
G_3SPS_6	–	–	–	–	–	–
S_4PSA_7	–	–	–	–	–	–
P_5SAQ_8	0.2	–	–	–	0.2	0.4
S_6AQD_9	29.9	–	–	–	3.2	53.1
A_7QDE_{10}	14.7	–	–	–	9.2	23.9
Q_8DEA_{11}	6.0	–	–	–	3.4	9.4
D_9EAS_{12}	9.7	–	–	–	2.8	12.5
$E_{10}ASP_{13}$	–	–	–	–	2.6	2.6
$A_{11}SPL_{14}$	–	–	–	–	–	–
$S_{12}PLS_{15}$	49.3	–	–	–	8.0	57.3
VGVAPG						
VGVA	7.8	–	–	18.8	–	26.6
GVAP	–	–	–	–	28.6	28.6
VAPG	–	–	–	–	–	–

CONCLUSIONS

Natural or pathogenic hydrolysis of the ECM proteins by peptidases yields small peptides, with major biological activity, which can enhance several pathologies. For instance, in tumoral cells, EDPs release MMPs, triggering both chemotactic and proliferative effects. ECM protein-derived peptides interact with cells via a cell-surface protein, the ELR, and more precisely via the 15-residue Sgal sequence of the EBP subunit. In this work, we propose a novel structural model, based on experimental and theoretical data, for the interaction between the Sgal peptide and several EDPs containing the GXXP motif, such as VGVAPG.

This structural study of the Sgal peptide shows the importance of the type I β-turn structure on the QDEA sequence. This structural motif is the most frequently observed throughout the MD simulations and its presence is characteristic of the lowest energy model obtained by MC calculations. This β-turn appears to have a key role in the anchoring process by exposing the Q residue to the solvent. Molecular docking computations confirm this assumption since all the best docking models show EDPs wrapping around the Q residue, thanks to a conformation exhibiting a type VIII β-turn structure on the GXXP motif. The latter observation supports our previous results showing the correlation between the presence of type VIII β-turn in the EDPs conformations and their ability to induce biological activities. The interaction between the Sgal peptide and EDPs is furthermore stabilized by three hydrogen bonds involving EDPs backbone

atoms, suggesting that central residues of the GXXP motif are not critical for binding to EBP.

The unraveling of the 3D structure of a molecular complex is a prerequisite to the understanding of the interaction mechanism between its components, and it is required in any attempt at complex modulation. These results open the way to the design of antagonists targeting the EBP to prevent the negative effects of ECM-derived peptides.

ACKNOWLEDGMENTS

Pr AJPA thanks Région Champagne Ardenne for providing a cluster of 20 PCs. SH and GM thank the Comité Calculateur de la Région Champagne Ardenne for sharing a part of the supercomputer resources. The authors are very grateful to Cédric Grauffel and Roland Stote for support with the REMD simulations and Aurélien Grosdidier, Vincent Zoete and Olivier Michielin for allowing the use of the EADock program. The authors thank referees for their helpful comments and Maryvonne Rosseneu for careful reading and correcting the manuscript.

REFERENCES

1. Rosenbloom J, Abrams WR, Mecham R. Extracellular matrix 4: the elastic fiber. FASEB J 1993;7:1208–1218.
2. Wrenn DS, Hinek A, Mecham RP. Kinetics of receptor-mediated binding of tropoelastin to ligament fibroblasts. J Biol Chem 1988;263:2280–2284.
3. Mecham RP, Hinek A, Entwistle R, Wrenn DS, Griffin GL, Senior RM. Elastin binds to a multifunctional 67-kilodalton peripheral membrane protein. Biochemistry 1989;28:3716–3722.
4. Hinek A, Wrenn DS, Mecham RP, Barondes SH. The elastin receptor: a galactoside-binding protein. Science 1988;239:1539–1541.
5. Hinek A, Rabinovitch M, Keeley F, Okamura-Oho Y, Callahan J. The 67-kD elastin/laminin-binding protein is related to an enzymatically inactive, alternatively spliced form of β-galactosidase. J Clin Invest 1993;91:1198–1205.
6. Hinek A, Rabinovitch M. 67-kD elastin-binding protein is a protective "companion" of extracellular insoluble elastin and intracellular tropoelastin. J Cell Biol 1994;126:563–574.
7. Hinek A, Keeley FW, Callahan J. Recycling of the 67-kDa elastin binding protein in arterial myocytes is imperative for secretion of tropoelastin. Exp Cell Res 1995;220:312–324.
8. Werb Z, Banda MJ, McKerrow JH, Sandhaus RA. Elastases and elastin degradation. J Invest Dermatol 1982;79 (Suppl 1):154s–159s.
9. Vrhovski B, Weiss AS. Biochemistry of tropoelastin. Eur J Biochem 1998;258:1–18.
10. Senior RM, Griffin GL, Mecham RP. Chemotactic activity of elastin-derived peptides. J Clin Invest 1980;66:859–862.
11. Varga Z, Jacob MP, Robert L, Fulop T, Jr. Identification and signal transduction mechanism of elastin peptide receptor in human leukocytes. FEBS Lett 1989;258:5–8.
12. Senior RM, Griffin GL, Mecham RP, Wrenn DS, Prasad KU, Urry DW. Val-Gly-Val-Ala-Pro-Gly, a repeating peptide in elastin, is chemotactic for fibroblasts and monocytes. J Cell Biol 1984;99:870–874.
13. Peterszegi G, Texier S, Robert L. Cell death by overload of the elastin-laminin receptor on human activated lymphocytes: protection by lactose and melibiose. Eur J Clin Invest 1999;29:166–172.
14. Tajima S, Wachi H, Uemura Y, Okamoto K. Modulation by elastin peptide VGVAPG of cell proliferation and elastin expression in human skin fibroblasts. Arch Dermatol Res 1997;289:489–492.
15. Lograno MD, Bisaccia F, Ostuni A, Daniele E, Tamburro AM. Identification of elastin peptides with vasorelaxant activity on rat thoracic aorta. Int J Biochem Cell Biol 1998;30:497–503.
16. Faury G, Garnier S, Weiss AS, Wallach J, Fulop T, Jr, Jacob MP, Mecham RP, Robert L, Verdetti J. Action of tropoelastin and synthetic elastin sequences on vascular tone and on free Ca^{2+} level in human vascular endothelial cells. Circ Res 1998;82:328–336.
17. Jacob MP, Hornebeck W, Lafuma C, Bernaudin JF, Robert L, Godeau G. Ultrastructural and biochemical modifications of rabbit arteries induced by immunization with soluble elastin peptides. Exp Mol Pathol 1984;41:171–190.
18. Jacob MP, Fulop T, Jr, Foris G, Robert L. Effect of elastin peptides on ion fluxes in mononuclear cells, fibroblasts, and smooth muscle cells. Proc Natl Acad Sci USA 1987;84:995–999.
19. Brassart B, Randoux A, Hornebeck W, Emonard H. Regulation of matrix metalloproteinase-2 (gelatinase A. MMP-2), membrane-type matrix metalloproteinase-1 (MT1-MMP) and tissue inhibitor of metalloproteinases-2 (TIMP-2) expression by elastin-derived peptides in human HT-1080 fibrosarcoma cell line. Clin Exp Metastasis 1998;16:489–500.
20. Huet E, Brassart B, Cauchard JH, Debelle L, Birembaut P, Wallach J, Emonard H, Polette M, Hornebeck W. Cumulative influence of elastin peptides and plasminogen on matrix metalloproteinase activation and type I collagen invasion by HT-1080 fibrosarcoma cells. Clin Exp Metastasis 2002;19:107–117.
21. Blood CH, Sasse J, Brodt P, Zetter BR. Identification of a tumor cell receptor for VGVAPG, an elastin-derived chemotactic peptide. J Cell Biol 1988;107:1987–1993.
22. Grosso LE, Scott M. PGAIPG, a repeated hexapeptide of bovine and human tropoelastin, is chemotactic for neutrophils and Lewis lung carcinoma cells. Arch Biochem Biophys 1993;305:401–404.
23. Blood CH, Zetter BR. Membrane-bound protein kinase C modulates receptor affinity and chemotactic responsiveness of Lewis lung carcinoma sublines to an elastin-derived peptide. J Biol Chem 1989;264:10614–10620.
24. Mecham RP, Hinek A, Griffin GL, Senior RM, Liotta LA. The elastin receptor shows structural and functional similarities to the 67-kDa tumor cell laminin receptor. J Biol Chem 1989;264:16652–16657.
25. Brassart B, Fuchs P, Huet E, Alix AJP, Wallach J, Tamburro AM, Delacoux F, Haye B, Emonard H, Hornebeck W, Debelle L. Conformational dependence of collagenase (matrix metalloproteinase-1) up-regulation by elastin peptides in cultured fibroblasts. J Biol Chem 2001;276:5222–5227.
26. Duffy MJ. Proteases as prognostic markers in cancer. Clin Cancer Res 1996;2:613–618.
27. Robinet A, Fahem A, Cauchard JH, Huet E, Vincent L, Lorimier S, Antonicelli F, Soria C, Crepin M, Hornebeck W, Bellon G. Elastin-derived peptides enhance angiogenesis by promoting endothelial cell migration and tubulogenesis through upregulation of MT1-MMP. J Cell Sci 2005;118 (Part 2):343–356.
28. Booms P, Ney A, Barthel F, Moroy G, Counsell D, Gille C, Guo G, Pregla R, Mundlos S, Alix AJ, Robinson PN. A fibrillin-1-fragment containing the elastin-binding-protein GxxPG consensus sequence upregulates matrix metalloproteinase-1: biochemical and computational analysis. J Mol Cell Cardiol 2006;40:234–246.
29. Rudenko G, Bonten E, d'Azzo A, Hol WG. Three-dimensional structure of the human 'protective protein': structure of the precursor form suggests a complex activation mechanism. Structure 1995;3:1249–1259.
30. Morreau H, Galjart NJ, Gillemans N, Willemsen R, van der Horst GT, d'Azzo A. Alternative splicing of β-galactosidase mRNA generates the classic lysosomal enzyme and a β-galactosidase-related protein. J Biol Chem 1989;264:20655–20663.

31. Privitera S, Prody CA, Callahan JW, Hinek A. The 67-kDa enzymatically inactive alternatively spliced variant of β-galactosidase is identical to the elastin/laminin-binding protein. J Biol Chem 1998;273:6319–6326.
32. Bisaccia F, Morelli MA, De Biasi M, Traniello S, Spisani S, Tamburro AM. Migration of monocytes in the presence of elastolytic fragments of elastin and in synthetic derivates. Structure-activity relationships. Int J Pept Protein Res 1994;44:332–341.
33. Castiglione Morelli MA, Bisaccia F, Spisani S, De Biasi M, Traniello S, Tamburro AM. Structure-activity relationships for some elastin-derived peptide chemoattractants. J Pept Res 1997;49:492–499.
34. Alix AJ. A turning point in the knowledge of the structure-function-activity relations of elastin. J Soc Biol 2001;195:181–193.
35. Fuchs P, Debelle L, Alix AJP. Structural study of some specific elastin hexapeptides activating MMP1. J Mol Struct 2001;565/566:335–339.
36. Fuchs PF, Alix AJ. High accuracy prediction of β-turns and their types using propensities and multiple alignments. Proteins 2005;59:828–839.
37. Floquet N, Hery-Huynh S, Dauchez M, Derreumaux P, Tamburro AM, Alix AJP. Structural characterization of VGVAPG, an elastin-derived peptide. Biopolymers 2004;76:266–280.
38. Fuchs PF, Bonvin AM, Bochicchio B, Pepe A, Alix AJ, Tamburro AM. Kinetics and thermodynamics of type VIII β-turn formation: a CD, NMR, and microsecond explicit molecular dynamics study of the GDNP tetrapeptide. Biophys J 2006;90:2745–2759.
39. Moroy G, Alix AJ, Hery-Huynh S. Structural characterization of human elastin derived peptides containing the GXXP sequence. Biopolymers 2005;78:206–220.
40. Wütrich K. NMR of proteins and nucleic acids. New York: Wiley; 1986. 320 p.
41. Altschul SF, Madden TL, Schaffer AA, Zhang J, Zhang Z, Miller W, Lipman DJ. Gapped BLAST and PSI-BLAST: a new generation of protein database search programs. Nucleic Acids Res 1997;25:3389–3402.
42. Thompson JD, Higgins DG, Gibson TJ. CLUSTAL W: improving the sensitivity of progressive multiple sequence alignment through sequence weighting, position-specific gap penalties and weight matrix choice. Nucleic Acids Res 1994;22:4673–4680.
43. Katona G, Wilmouth RC, Wright PA, Berglund GI, Hajdu J, Neutze R, Schofield CJ. X-ray structure of a serine protease acyl-enzyme complex at 0.95-A resolution. J Biol Chem 2002;277:21962–21970.
44. Schaumann T, Braun W, Wuthrich K. The program FANTOM for energy refinement of polypeptides and proteins using a Newton–Raphson minimizer in torsion angle space. Biopolymers 1990;29:679–694.
45. Abe H, Braun W, Noguti T, Go N. Rapid calculation of first and second derivatives of conformational energy with respect to dihedral angles for proteins. General recurrent equations. Comput Chem 1984;8:239–247.
46. von Freyberg B, Braun W. Efficient search for all low energy conformations of polypeptides by Monte Carlo methods. J Comput Chem 1993;12:1065–1076.
47. Metropolis N, Rosenbluth AW, Rosenbluth MN, Teller AH, Teller E. Equation of state calculations by fast computing machines. J Phys Chem 1953;99:1087–1092.
48. Efremov RG, Nolde DE, Vergoten G, Arseniev AS. A solvent model for simulations of peptides in bilayers. I. Membrane-promoting α-helix formation. Biophys J 1999;76:2448–2459.
49. Brooks BR, Bruccoleri BD, Olafson BD, States DJ, Swaminathan S, Karplus M. CHARMM: a program for macromolecular energy, minimization and dynamics calculations. J Comput Chem 1983;4:187–217.
50. MacKerrel ADJ, Bashford D, Bellott M, Dunbrack RLJ, Evanseck JD, Field MJ, Fisher S, Gao J, Guo SH, Ha S, Joseph-MacCarthy D, Kuchnir L, Kuczera K, Lau FTK, Mattos C, Michnick S, Ngo T, Nguyen DT, Prodhom B, Reiher WEI, Roux B, Schlenkrich M, Smith JC, Stote R, Straub J, Watanabe M, Wiorkiewicz-Kuczera J, Yin D, Karplus M. All-atom potential for molecular modeling and dynamics studies of proteins. J Phys Chem B 1998;102:3586–3616.
51. Steinbach PJ, Brooks BR. New spherical-cutoff methods for long-range forces in macromolecular simulation. J Comput Chem 1994;15:667–683.
52. Jorgensen WL, Chandarsekhar J, Madura JD, Impey RW, Klein ML. Comparison of simple potential functions for simulating water. J Chem Phys 1983;79:926–935.
53. Brooks BR, Karplus M, Pettitt BM. Protein: a theoretical perspective of dynamics, structure and thermodynamics (Advances in chemical physics). New York: Wiley-Interscience; 1988.
54. Frishman D, Argos P. Knowledge-based secondary structure assignment. Proteins 1995;23:566–579.
55. Derreumaux P. A diffusion process-controlled Monte Carlo method for finding the global energy minimum of the polypeptide chain. I. Formulation and test on a hexadecapeptide. J Chem Phys 1997;106:5260–5270.
56. Morris GM, Goodsell DS, Halliday RS, Huey R, Hart WE, Belew RK, Olson AJ. Automated docking using a Lamarckian genetic algorithm and an empirical binding free energy function. J Comput Chem 1998;19:1639–1662.
57. Drake AF, Siligardi G, Gibbons WA. Reassessment of the electronic circular dichroism criteria for random coil conformations of poly(L-lysine) and the implications for protein folding and denaturation studies. Biophys Chem 1988;31:143–146.
58. Shi Z, Olson CA, Rose GD, Baldwin RL, Kallenbach NR. Polyproline II structure in a sequence of seven alanine residues. Proc Natl Acad Sci USA 2002;99:9190–9195.
59. Shi Z, Woody RW, Kallenbach NR. Is polyproline II a major backbone conformation in unfolded proteins? Adv Protein Chem 2002;62:163–240.
60. Karplus M. Contact electron-spin coupling of nuclear magnetic moments. J Phys Chem 1959;30:11–15.
61. Navia MA, McKeever BM, Springer JP, Lin TY, Williams HR, Fluder EM, Dorn CP, Hoogsteen K. Structure of human neutrophil elastase in complex with a peptide chloromethyl ketone inhibitor at 1.84-A resolution. Proc Natl Acad Sci USA 1989;86:7–11.
62. Berglund GI, Willassen NP, Hordvik A, Smalas AO. Structure of native pancreatic elastase from North Atlantic salmon at 1.61 A resolution. Acta Crystallogr D Biol Crystallogr 1995;51 (Part 6):925–937.
63. Hutchinson EG, Thornton JM. A revised set of potentials for β-turn formation in proteins. Protein Sci 1994;3:2207–2216.
64. MacArthur MW, Thornton JM. Influence of proline residues on protein conformation. J Mol Biol 1991;218:397–412.
65. Sugita Y, Okamoto Y. Replica-exchange molecular dynamics method for protein folding. Chem Phys Lett 1999;314:141–151.
66. Bisaccia F, Ostuni A, Tamburro AM. Biological activities of elastin peptides. Curr Top Pept Protein Res 1999;44:332–341.
67. Grosdidier A, Zoete V, Michielin O. EADock: docking of small molecules into protein active sites with a multiobjective evolutionary optimization. Proteins 2007;67:1010–1025.